

SAR COMPLIANCE TESTING OF PROXIM CORPORATION MODEL 8460  
(FCC ID# HZB-8460) CARDBUS CARD INSERTED INTO  
A LAPTOP COMPUTER

August 12, 2002

Submitted to: Mr. Nathan Mueller  
Design Engineer  
Proxim Corporation Inc.  
71 North 490 West  
American Fork, UT 84003

Submitted by: Om P. Gandhi  
Professor of Electrical and Computer Engineering  
University of Utah  
50 S Central Campus Dr., Rm. 3280  
Salt Lake City, UT 84112-9206

SAR COMPLIANCE TESTING OF PROXIM CORPORATION MODEL 8460  
(FCC ID# HZB-8460) CARDBUS CARD INSERTED INTO  
A LAPTOP COMPUTER

**I. Introduction**

The U.S. Federal Communications Commission (FCC) has adopted limits of human exposure to RF emissions from mobile and portable devices that are regulated by the FCC [1]. The FCC has also issued Supplement C (Edition 97-01) to OET Bulletin 65 [2] and a more recent version of the same [3] defining both the measurement and the computational procedures that should be followed for evaluating compliance of mobile and portable devices with FCC limits for human exposure to radiofrequency emissions.

We have used the measurement procedure for SAR compliance testing of the Proxim Corporation Model 8460 CardBus Card inserted into a laptop computer. A photograph of the unit with the CardBus Card inserted into the laptop computer is given in Fig. 1. A picture of the Model 8460 CardBus Card placed on the laptop is given in Fig. 2. The Proxim Model 8460 CardBus Card operates with a nominal conducted RF power output of 20 dBm (100 mW) for the frequency band 5.18-5.85 GHz.

For SAR measurements, two configurations of the wireless PC relative to the experimental phantom have been used:

- a. Since the wireless PC may possibly be placed on a user's lap where the RF antennas would be the closest to the body, a planar phantom model with inside dimensions 12"  $\times$  16.5" (30.5  $\times$  41.9 cm) and a base thickness of  $2.0 \pm 0.2$  mm (recommended in [3]) was used for SAR measurements and the wireless PC cards mounted in a portable computer (as in Fig. 1) pressed against the bottom of this phantom (see Fig. 3).
- b. For a bystander, the "end-on" SAR value is obtained for the PC and the card edge at 90° to the flat phantom with a spacing of 2.5 cm (see Fig. 4).

## II. Experimental Measurements of SAR Distribution

As aforementioned, the measurements of the SAR distributions for the Proxim Model 8460 CardBus Card inserted into a laptop computer (as in Fig. 1), both for the "above-lap" and "end-on" positions, were done with a planar rectangular box phantom made of acrylic of inside dimensions 12"  $\times$  16.5" (30.5  $\times$  41.9 cm) shown in Figs. 3 and 4 for "above-lap" and "end-on" positions, respectively. This box phantom of external dimensions 13"  $\times$  17.5" (33  $\times$  44.5 cm) is filled with a tissue-simulant fluid up to a depth of 15 cm. As recommended in [3], the base thickness of the box phantom is  $2.0 \pm 0.2$  mm (0.079"). As seen in Figs. 3 and 4, a 1" thick Styrofoam block is used under the base, except for the region of the wireless laptop to prevent bending of the 2 mm thin base. Also for the SAR testing for the "end-on" position, a separation of 1" (2.5 cm) from the end of the PC card to the bottom of the planar phantom is used.

The tissue-simulant fluid uses a composition developed at the University of Utah which consists of 68.0% water, 31.0% sugar and 1% HEC. For this composition, we have measured the dielectric properties using a Hewlett Packard (HP) Model 85070B Dielectric Probe in conjunction with HP Model 8720C Network Analyzer (50 MHz-20 GHz). The measured dielectric properties at a mid band frequency of 5.30 GHz are as follows:  $\epsilon_r = 48.5 \pm 1.7$  and  $\sigma = 5.40 \pm 0.08$  S/m. From the FCC Supplement C [3], we obtain the desired dielectric properties to simulate the body tissue at the midband frequency of 5.30 GHz to be  $\epsilon_r = 48.9$  and  $\sigma = 5.42$  S/m. Thus, the measured properties for the body-simulant fluid are close to the desired values.

## III. Calibration of the E-Field Probe

Supplement C, Appendix D does not spell out a detailed procedure to use for system verification and electric field calibration for frequencies above 3000 MHz. However, the IEEE Draft Standard P1528 [4] does suggest a recommended procedure for probe calibration (see Section 4.4.1 of [4]) for frequencies above 800 MHz where waveguide size is manageable. Calibration using a rectangular waveguide is recommended. As in some previously reported SAR measurements at 6 GHz [5], we have calibrated the Narda Model 8021 Miniature

Broadband Electric Field Probe of tip diameter 4 mm (internal dipole dimensions on the order of 2.5 mm) using a rectangular waveguide WR 159 (of internal dimensions  $1.590 \times 0.795$  inches) that was filled with the tissue-simulant fluid of composition given in Section II. The triaxial (3 dipole) E-field probe was originally developed by Howard Bassen and colleagues of FDA and has been manufactured under license by Narda Microwave Corporation, Hauppauge, New York. The probe is described in detail in references 6 and 7. It uses three orthogonal pick up dipoles each of length about 2.5 mm with their own leadless zero voltage Schottky barrier diodes operating in the square law region. The sum of the three diode outputs read by three microvoltmeters [8] gives an output proportional to  $E^2$ .

As suggested in the Draft Standard P1526, the waveguide (WR 159) filled with the tissue-simulant fluid was maintained vertically. From microwave field theory [see e.g. ref. 9], the transverse field distribution in the liquid corresponds to the fundamental mode ( $TE_{10}$ ) with an exponential decay in the vertical direction ( $z$ -axis). The liquid level was 15 cm deep which is deep enough to guarantee that reflections from the top liquid surface do not affect the calibration. By comparing the square of the decaying electric fields expected in the tissue from the analytical expressions for the  $TE_{10}$  mode of the rectangular waveguide, we obtained a calibration factor of  $2.98 \text{ (mW/kg)/}\mu\text{V}$  with a variability of less than  $\pm 2\%$  for measurement frequencies of 5.2, 5.3, 5.7, and 5.8 GHz, respectively.

The data for the calibration of the E-field probe closest to the SAR tests given here was August 8, 2002.

#### **IV. The Measured SAR Distributions**

The SAR distributions were determined using the automated SAR measurement system developed at the University of Utah ([8] -- attached here as Appendix A). As described in [8], this SAR measurement system has been validated using a number of wireless telephones at 835 and 1900 MHz, respectively.

The highest SAR region for each of the measurement frequencies (5.18, 5.32, 5.745, and 5.825 GHz) was identified in the first instance by using a coarser sampling with a step size of 8.0 mm over three overlapping areas for a total scan area of  $8.0 \times 9.6$  cm. After identifying the region of the highest SAR, the SAR distribution was measured with a resolution of 2 mm in order to obtain the peak  $1 \text{ cm}^3$  or 1-g SAR. The SAR measurements are performed at 4, 6, 8, 10, 12 mm height from the bottom surface of the body-simulant fluid. The SARs thus measured were extrapolated using a second-order least-square fit to the measured data to obtain values at 1, 3, 5, 7 and 9 mm height and used to obtain 1-g SARs. The uncertainty analysis of the University of Utah SAR measurement system is given in Appendix B. The combined standard uncertainty is  $\pm 8.3\%$ .

For each of the SAR measurements, we used the FCC-recommended channel power spectrum analyzer method. Using the Hewlett Packard Model HP8592B Spectrum Analyzer, the power before and after making the SAR measurements was found to be within 0.5 dB.

The z-axis scan plots taken at the highest SAR locations for each test are given in Figs. 5 and 6, respectively.

The detailed SAR distributions measured with a stepper-motor-controlled step size of 2 mm for transmit frequencies of 5.18, 5.32, 5.745, and 5.845 GHz are given in Tables 1-4 for the "above-lap" position and in Tables 5-8 for the "end-on" position, respectively. The SARs are given for xy planes at heights z of 1, 3, 5, 7, and 9 mm for each of the placements of the PC card relative to the flat phantom. The individual SAR values for this grid of  $5 \times 5 \times 5$  or 125 points are averaged to obtain the peak 1-g SAR values (for a volume of  $1 \text{ cm}^3$ ). For the measurements in Tables 1-4, the separation between the Proxim Model 8460 CardBus Card and the bottom of the experimental phantom is on the order of 1 cm. For the "end-on" position, the separation between the card edge at  $90^\circ$  to the bottom of the flat phantom is 2.5 cm and the SAR distributions at the various frequencies are given in Tables 5-8. The peak 1-g SARs for various configurations of the CardBus card are summarized in Table 9. It may be noted that all of the measured 1-g SARs are less than the FCC96-326 Guideline of 1.6 W/kg.

## **V. Comparison of the Data With FCC 96-326 Guidelines**

According to the FCC 96-326 Guideline [1], the peak SAR for any 1-g of tissue should not exceed 1.6 W/kg. For the maximum radiated power condition of 20 dBm (100 mW), the Proxim Model 8460 CardBus Card has been measured to give peak 1-g SARs of 0.22 to 0.82W/kg which are smaller than 1.6 W/kg.

## REFERENCES

1. Federal Communications Commission, "Guidelines for Evaluating the Environmental Effects of Radiofrequency Radiation," FCC 96-326, August 1, 1996.
2. K. Chan, R. F. Cleveland, Jr., and D. L. Means, "Evaluating Compliance With FCC Guidelines for Human Exposure to Radiofrequency Electromagnetic Fields," Supplement C (Edition 97-01) to OET Bulletin 65, December, 1997. Available from Office of Engineering and Technology, Federal Communications Commission, Washington D.C., 20554.
3. Federal Communications Commission "Supplement C Edition 01-01 to OET Bulletin 65 Edition 97-01" June 2001.
4. IEEE Draft Standard P1528, "Recommended Practice for Determining the Peak Spatial-Average Specific Absorption Rate (SAR) in the Human Body Due to Wireless Communication Devices: Experimental Techniques," Draft CBD1.0, April 4, 2002 (IEEE Standards Coordinating Committee 34).
5. O. P. Gandhi and J-Y. Chen, "Electromagnetic Absorption in the Human Head from Experimental 6-GHz Handheld Transceivers," *IEEE Transactions on Electromagnetic Compatibility*, Vol. 39(4), pp. 547-558, 1995.
6. H. Bassen. M. Swicord, and J. Abita, "A Miniature Broadband Electric Field Probe," *Ann. New York Academy of Sciences*, Vol. 247, pp. 481-493, 1974.
7. H. Bassen and T. Babij, "Experimental Techniques and Instrumentation," Chapter 7 in *Biological Effects and Medical Applications of Electromagnetic Energy*, O. P. Gandhi, Editor, Prentice Hall Inc., Englewood Cliffs, NJ, 1990.
8. Q. Yu, O. P. Gandhi, M. Aronsson, and D. Wu, "An Automated SAR Measurement System for Compliance Testing of Personal Wireless Devices," *IEEE Transactions on Electromagnetic Compatibility*, Vol. 41(3), pp. 234-245, August 1999 (attached as Appendix A).
9. O. P. Gandhi, *Microwave Engineering and Applications*, Pergamon Press, New York, 1981.

Table 1. **Above-lap position.** The SARs measured for the Proxim Model 8460 CardBus Card (nominal conducted power of 20 dBm) inserted into a laptop computer at 5.18 GHz

**1-g SAR = 0.667 W/kg**

**a. At depth of 1 mm**

1.345	1.507	1.532	1.558	1.373
1.407	1.464	1.598	1.574	1.387
1.400	1.451	1.505	1.489	1.346
1.342	1.420	1.440	1.354	1.203
1.244	1.379	1.406	1.332	1.181

**b. At depth of 3 mm**

0.905	1.001	1.024	1.033	0.911
0.940	0.981	1.070	1.037	0.909
0.933	0.969	0.994	0.981	0.886
0.890	0.955	0.948	0.893	0.800
0.824	0.921	0.938	0.900	0.848

**c. At depth of 5 mm**

0.554	0.601	0.622	0.619	0.544
0.571	0.597	0.651	0.614	0.533
0.564	0.585	0.592	0.582	0.524
0.532	0.583	0.560	0.528	0.480
0.494	0.561	0.571	0.564	0.586

**d. At depth of 7 mm**

0.292	0.308	0.326	0.317	0.271
0.299	0.313	0.342	0.306	0.258
0.292	0.299	0.300	0.290	0.260
0.269	0.303	0.276	0.259	0.241
0.256	0.299	0.306	0.324	0.397

**e. At depth of 9 mm**

0.119	0.121	0.136	0.126	0.092
0.125	0.128	0.143	0.113	0.084
0.118	0.111	0.118	0.107	0.093
0.099	0.116	0.098	0.086	0.085
0.108	0.135	0.141	0.180	0.279



Table 2. **Above-lap position.** The SARs measured for the Proxim Model 8460 CardBus Card (nominal conducted power of 20 dBm) inserted into a laptop computer at 5.32 GHz

**1-g SAR = 0.816 W/kg**

**a. At depth of 1 mm**

1.632	1.741	1.781	1.755	1.649
1.712	1.798	1.852	1.818	1.727
1.738	1.847	1.859	1.845	1.678
1.738	1.845	1.869	1.812	1.659
1.646	1.771	1.811	1.787	1.692

**b. At depth of 3 mm**

1.078	1.149	1.163	1.145	1.069
1.135	1.183	1.216	1.192	1.123
1.141	1.218	1.218	1.208	1.097
1.141	1.211	1.222	1.191	1.093
1.084	1.165	1.194	1.185	1.139

**c. At depth of 5 mm**

0.642	0.684	0.679	0.668	0.617
0.681	0.701	0.719	0.702	0.652
0.673	0.723	0.716	0.708	0.642
0.673	0.715	0.716	0.704	0.647
0.643	0.690	0.710	0.714	0.706

**d. At depth of 7 mm**

0.324	0.347	0.330	0.323	0.292
0.350	0.353	0.356	0.348	0.315
0.336	0.363	0.353	0.345	0.313
0.336	0.355	0.351	0.350	0.322
0.322	0.345	0.359	0.375	0.396

**e. At depth of 9 mm**

0.125	0.136	0.116	0.110	0.095
0.142	0.138	0.133	0.131	0.111
0.128	0.138	0.129	0.120	0.109
0.128	0.133	0.127	0.130	0.118
0.123	0.130	0.140	0.167	0.206

Table 3. **Above-lap position.** The SARs measured for the Proxim Model 8460 CardBus Card (nominal conducted power of 20 dBm) inserted into a laptop computer at 5.745 GHz

**1-g SAR = 0.761 W/kg**

**a. At depth of 1 mm**

1.380	1.492	1.541	1.568	1.497
1.516	1.633	1.706	1.711	1.644
1.555	1.709	1.791	1.766	1.688
1.518	1.686	1.762	1.776	1.690
1.428	1.581	1.675	1.699	1.637

**b. At depth of 3 mm**

0.910	0.982	1.024	1.029	0.989
0.997	1.077	1.124	1.134	1.086
1.031	1.123	1.180	1.168	1.115
1.001	1.108	1.157	1.172	1.111
0.943	1.043	1.106	1.124	1.091

**c. At depth of 5 mm**

0.541	0.583	0.617	0.607	0.590
0.591	0.642	0.668	0.682	0.649
0.620	0.667	0.701	0.699	0.666
0.597	0.659	0.686	0.699	0.657
0.564	0.622	0.661	0.675	0.665

**d. At depth of 7 mm**

0.275	0.296	0.321	0.303	0.300
0.300	0.328	0.339	0.354	0.332
0.322	0.336	0.356	0.359	0.340
0.305	0.336	0.346	0.357	0.330
0.291	0.319	0.341	0.353	0.359

**e. At depth of 9 mm**

0.111	0.120	0.136	0.117	0.120
0.123	0.136	0.137	0.150	0.136
0.138	0.135	0.144	0.147	0.138
0.125	0.141	0.139	0.147	0.128
0.124	0.135	0.145	0.158	0.174

Table 4. **Above-lap position.** The SARs measured for the Proxim Model 8460 CardBus Card (nominal conducted power of 20 dBm) inserted into a laptop computer at 5.825 GHz

**1-g SAR = 0.653 W/kg**

**a. At depth of 1 mm**

1.292	1.363	1.434	1.397	1.309
1.391	1.496	1.506	1.535	1.416
1.377	1.500	1.540	1.537	1.474
1.347	1.487	1.534	1.518	1.420
1.282	1.401	1.471	1.476	1.432

**b. At depth of 3 mm**

0.839	0.885	0.937	0.901	0.835
0.905	0.980	0.982	0.992	0.914
0.905	0.980	0.997	0.995	0.952
0.881	0.962	0.993	0.993	0.923
0.837	0.916	0.966	0.982	0.960

**c. At depth of 5 mm**

0.484	0.511	0.546	0.513	0.465
0.524	0.574	0.570	0.568	0.522
0.533	0.571	0.572	0.571	0.543
0.515	0.552	0.571	0.580	0.534
0.489	0.536	0.571	0.596	0.592

**d. At depth of 7 mm**

0.227	0.241	0.261	0.234	0.199
0.248	0.278	0.272	0.264	0.240
0.261	0.273	0.265	0.267	0.249
0.249	0.258	0.268	0.279	0.251
0.238	0.262	0.287	0.316	0.326

**e. At depth of 9 mm**

0.068	0.075	0.082	0.064	0.037
0.077	0.092	0.087	0.079	0.068
0.090	0.087	0.077	0.082	0.069
0.083	0.078	0.084	0.090	0.076
0.084	0.095	0.112	0.144	0.164

Table 5. **End-on position.** The SARs measured for the Proxim Model 8460 CardBus Card (nominal conducted power of 20 dBm) inserted into a laptop computer at 5.18 GHz. Distance to the bottom of the flat phantom = 2.5 cm.

**1-g SAR = 0.218 W/kg**

**a. At depth of 1 mm**

0.419	0.436	0.419	0.464	0.510
0.483	0.454	0.525	0.500	0.393
0.496	0.454	0.485	0.456	0.517
0.392	0.423	0.487	0.468	0.456
0.471	0.497	0.496	0.535	0.595

**b. At depth of 3 mm**

0.277	0.283	0.277	0.301	0.343
0.325	0.314	0.350	0.321	0.269
0.308	0.299	0.317	0.307	0.326
0.250	0.289	0.306	0.312	0.286
0.299	0.323	0.329	0.372	0.424

**c. At depth of 5 mm**

0.164	0.162	0.164	0.175	0.211
0.198	0.201	0.210	0.181	0.170
0.164	0.175	0.183	0.185	0.175
0.137	0.178	0.163	0.185	0.152
0.165	0.186	0.197	0.243	0.250

**d. At depth of 7 mm**

0.081	0.073	0.081	0.087	0.115
0.103	0.115	0.105	0.081	0.094
0.063	0.083	0.082	0.092	0.067
0.053	0.091	0.061	0.088	0.053
0.069	0.087	0.101	0.148	0.121

**e. At depth of 9 mm**

0.027	0.015	0.027	0.036	0.054
0.040	0.057	0.037	0.021	0.041
0.005	0.022	0.014	0.026	0.001
0.000	0.028	0.003	0.020	0.010
0.009	0.025	0.041	0.086	0.049

Table 6.

**End-on position.** The SARs measured for the Proxim Model 8460 CardBus Card (nominal conducted power of 20 dBm) inserted into a laptop computer at 5.32 GHz. Distance to the bottom of the flat phantom = 2.5 cm.

$$1\text{-g SAR} = 0.317 \text{ W/kg}$$

**a. At depth of 1 mm**

0.642	0.651	0.635	0.616	0.599
0.684	0.629	0.616	0.644	0.601
0.655	0.640	0.664	0.636	0.635
0.630	0.636	0.663	0.649	0.657
0.656	0.647	0.661	0.679	0.657

**b. At depth of 3 mm**

0.435	0.441	0.434	0.422	0.416
0.461	0.424	0.415	0.432	0.407
0.444	0.437	0.446	0.433	0.430
0.428	0.429	0.446	0.446	0.440
0.444	0.438	0.450	0.459	0.448

**c. At depth of 5 mm**

0.272	0.277	0.275	0.270	0.269
0.285	0.262	0.257	0.265	0.254
0.278	0.276	0.275	0.273	0.268
0.267	0.266	0.277	0.284	0.271
0.277	0.274	0.285	0.287	0.286

**d. At depth of 7 mm**

0.153	0.159	0.156	0.159	0.159
0.157	0.144	0.142	0.145	0.141
0.156	0.158	0.151	0.154	0.150
0.147	0.147	0.153	0.164	0.147
0.157	0.155	0.166	0.163	0.173

**e. At depth of 9 mm**

0.078	0.086	0.079	0.089	0.086
0.076	0.068	0.070	0.069	0.068
0.079	0.081	0.075	0.078	0.076
0.069	0.072	0.076	0.084	0.070
0.081	0.083	0.092	0.087	0.108

Table 7. **End-on position.** The SARs measured for the Proxim Model 8460 CardBus Card (nominal conducted power of 20 dBm) inserted into a laptop computer at 5.745 GHz. Distance to the bottom of the flat phantom = 2.5 cm.

**1-g SAR = 0.274 W/kg**

**a. At depth of 1 mm**

0.472	0.470	0.502	0.482	0.511
0.550	0.531	0.471	0.552	0.530
0.512	0.501	0.567	0.496	0.524
0.478	0.522	0.573	0.597	0.542
0.556	0.562	0.575	0.564	0.585

**b. At depth of 3 mm**

0.334	0.340	0.345	0.328	0.350
0.366	0.363	0.337	0.380	0.364
0.346	0.344	0.376	0.352	0.363
0.333	0.368	0.394	0.416	0.379
0.386	0.389	0.393	0.404	0.424

**c. At depth of 5 mm**

0.225	0.234	0.221	0.208	0.223
0.225	0.232	0.232	0.245	0.234
0.216	0.220	0.230	0.234	0.234
0.219	0.245	0.255	0.274	0.250
0.254	0.253	0.252	0.276	0.299

**d. At depth of 7 mm**

0.144	0.152	0.131	0.122	0.132
0.128	0.138	0.155	0.148	0.140
0.121	0.129	0.127	0.141	0.137
0.136	0.153	0.154	0.170	0.155
0.158	0.154	0.152	0.181	0.210

**e. At depth of 9 mm**

0.093	0.092	0.073	0.070	0.076
0.074	0.080	0.107	0.089	0.082
0.062	0.072	0.068	0.075	0.070
0.083	0.091	0.091	0.105	0.095
0.100	0.092	0.092	0.118	0.158

Table 8. **End-on position.** The SARs measured for the Proxim Model 8460 CardBus Card (nominal conducted power of 20 dBm) inserted into a laptop computer at 5.825 GHz. Distance to the bottom of the flat phantom = 2.5 cm.

**1-g SAR = 0.310 W/kg**

**a. At depth of 1 mm**

0.532	0.599	0.578	0.578	0.577
0.592	0.497	0.639	0.605	0.667
0.601	0.638	0.618	0.616	0.625
0.616	0.652	0.599	0.632	0.605
0.579	0.585	0.609	0.640	0.630

**b. At depth of 3 mm**

0.376	0.410	0.395	0.395	0.394
0.402	0.375	0.448	0.425	0.456
0.416	0.433	0.428	0.437	0.424
0.419	0.445	0.423	0.433	0.412
0.401	0.398	0.420	0.434	0.436

**c. At depth of 5 mm**

0.251	0.261	0.251	0.251	0.251
0.254	0.268	0.297	0.284	0.291
0.271	0.274	0.279	0.293	0.267
0.266	0.285	0.282	0.276	0.261
0.260	0.252	0.271	0.273	0.284

**d. At depth of 7 mm**

0.160	0.153	0.145	0.14	0.148
0.147	0.174	0.184	0.179	0.171
0.168	0.160	0.172	0.185	0.155
0.158	0.169	0.177	0.161	0.151
0.157	0.148	0.163	0.158	0.177

**e. At depth of 9 mm**

0.100	0.085	0.077	0.077	0.083
0.081	0.095	0.112	0.112	0.097
0.107	0.091	0.106	0.112	0.087
0.095	0.099	0.107	0.086	0.082
0.091	0.085	0.095	0.088	0.112

Table 9. The peak 1-g SARs measured for the Proxim Model 8460 CardBus Card (nominal conducted power of 20 dBm) inserted into a laptop computer.

**1-g SAR in W/kg**

PC position relative to the flat phantom	Spacing to the bottom of the phantom	5.18 GHz	5.32 GHz	5.745 GHz	5.825 GHz
“Above-lap”: bottom of PC pressed against bottom of the flat phantom	1 cm	0.667	0.816	0.761	0.653
“End-on”: card edge at 90° relative to the bottom of the flat phantom	2.5 cm	0.218	0.317	0.274	0.310



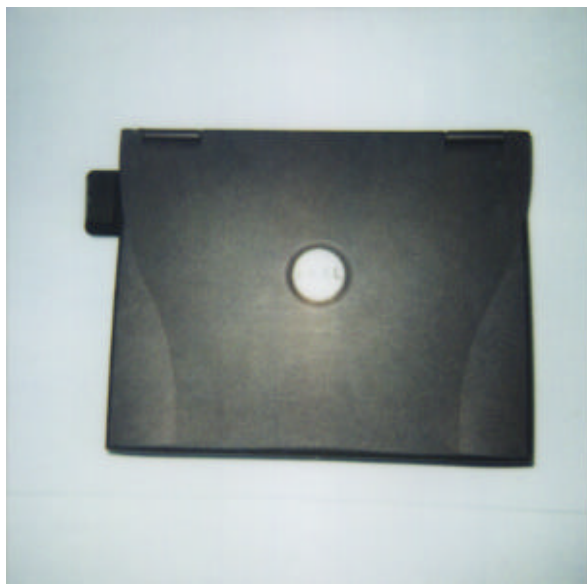


Fig. 1. Photograph of the Proxim Model 8460 CardBus Card inserted into a laptop computer.



Fig. 2. A picture of the Proxim Model 8460 CardBus Card placed on the laptop computer.

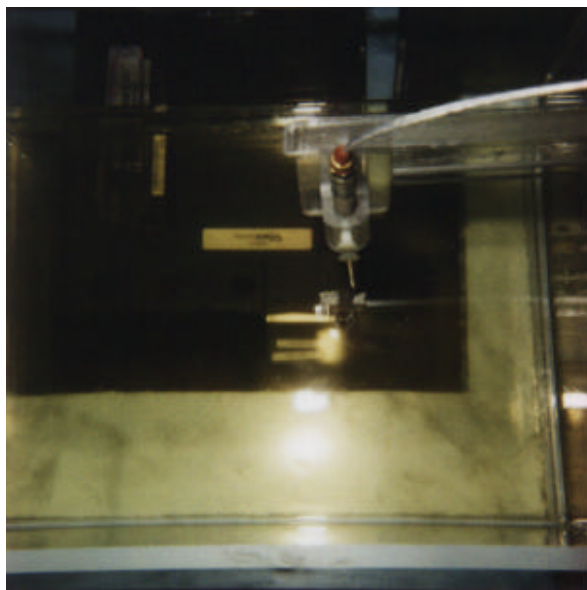


Fig. 3. Photograph of the Proxim Model 8460 CardBus Card inserted into a laptop computer with its bottom pressed against the bottom of the planar tissue-simulant phantom to simulate "above-lap" placement of the wireless PC. A Styrofoam block is used under the base to prevent bending of the 2 mm thin base of the phantom.

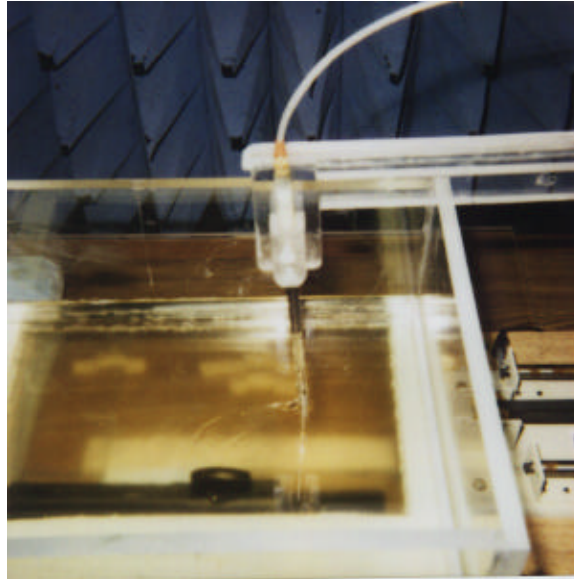


Fig. 4. Photograph of the Proxim Model 8460 CardBus Card inserted into a portable computer (as in Fig. 1) placed with the card edge at  $90^\circ$  and separated from the bottom of the phantom by 2.5 cm for "end-on" testing of SAR. As in Fig. 3, here too, a Styrofoam block is used under the base to prevent bending of the 2 mm thin base of the phantom.

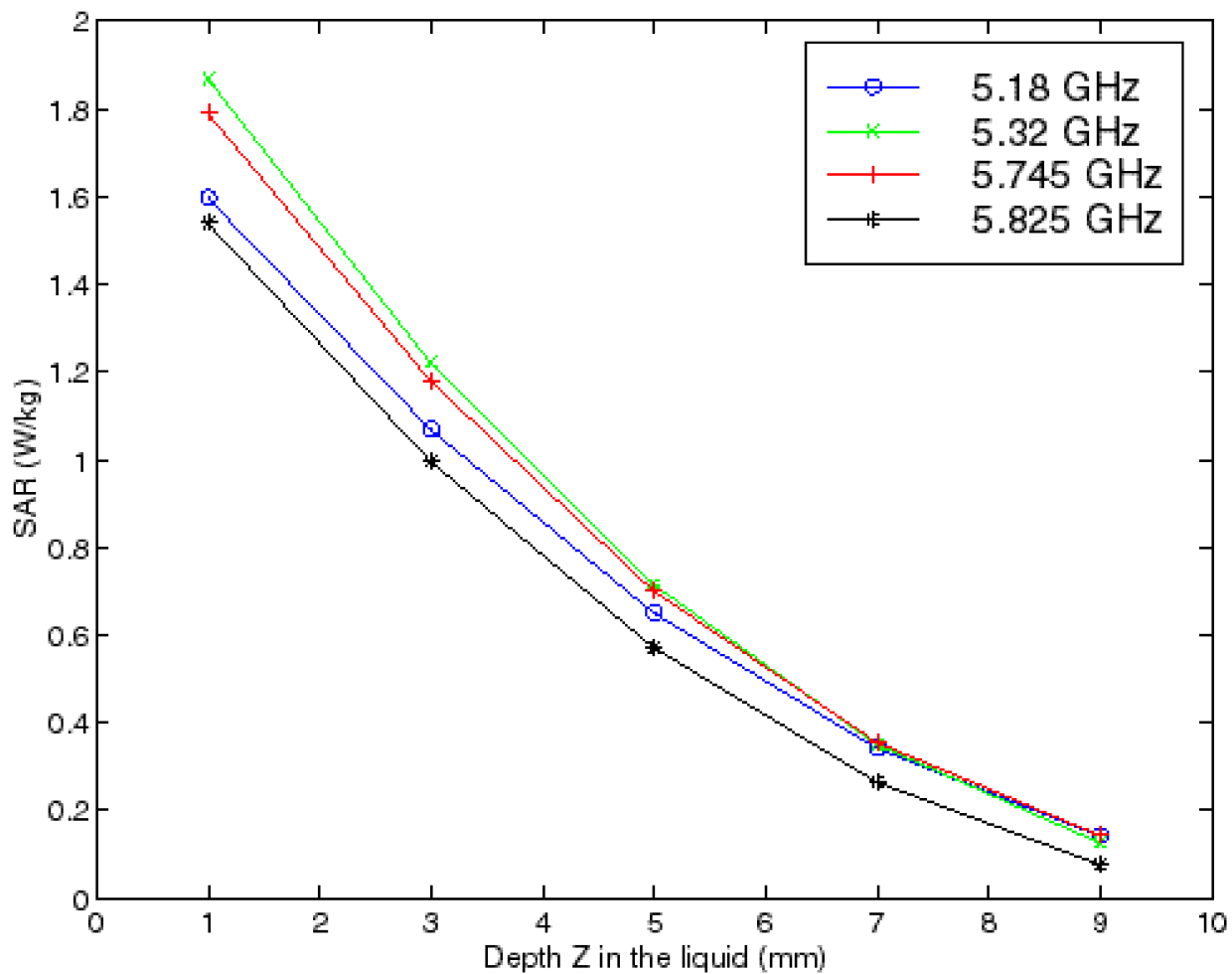


Fig. 5. Plot of the SAR variations as a function of depth Z in the liquid for locations of highest SAR (from Tables 1-4 -- Above-lap position) for Proxim Model 8460 CardBus Card.

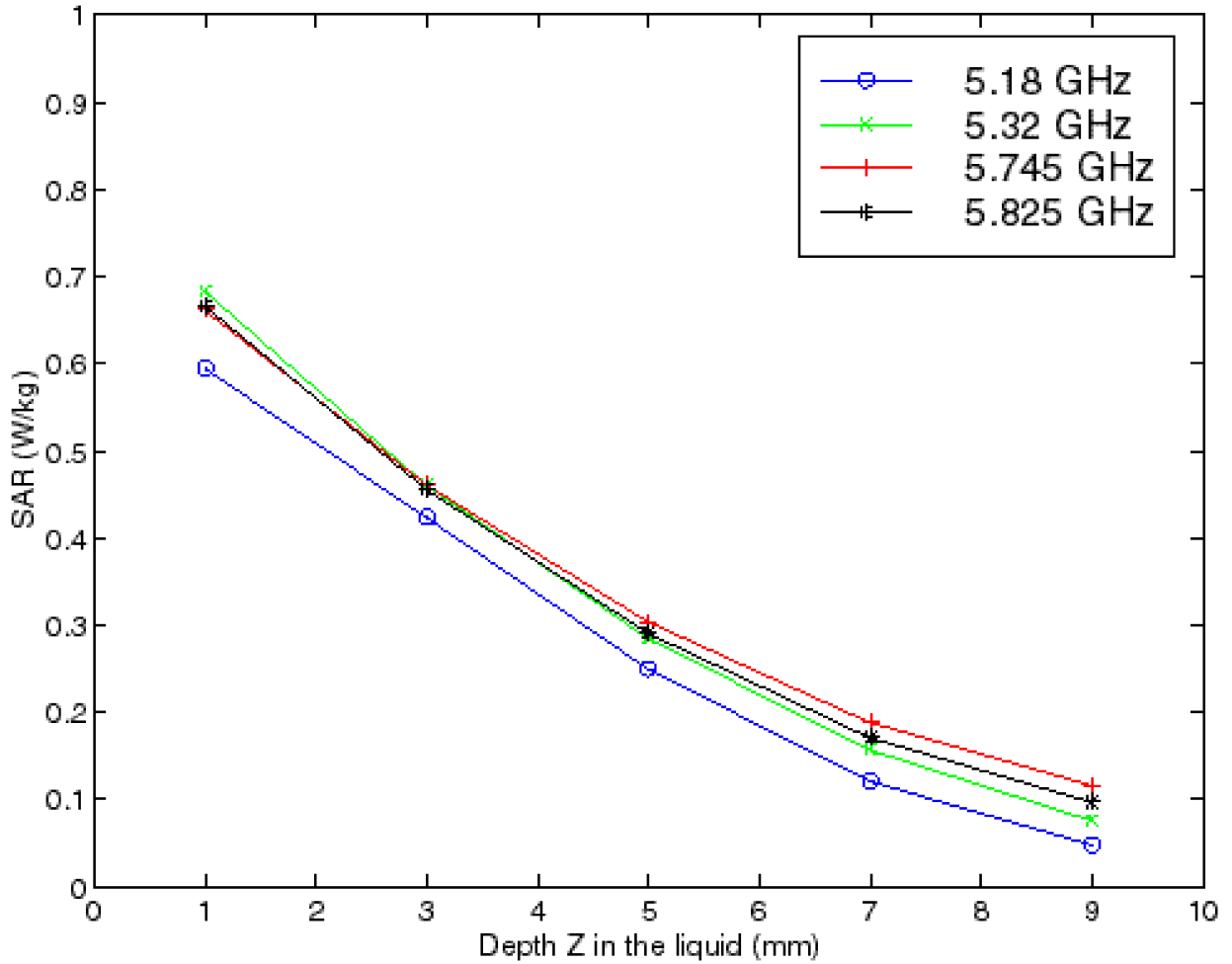


Fig. 6. Plot of the SAR variations as a function of depth Z in the liquid for locations of highest SAR (from Tables 5-8 -- End-on position) for Proxim Model 8460 CardBus Card.

# An Automated SAR Measurement System for Compliance Testing of Personal Wireless Devices

Qishan Yu, Om P. Gandhi, *Life Fellow, IEEE*, Magnus Aronsson, *Student Member, IEEE*, and Ding Wu

**Abstract**—An automated specific absorption rate (SAR) measurement system has been developed for compliance testing of personal wireless devices. Unlike other systems, this system uses a model with a lossy ear-shaped protrusion and the accuracy of this experimental setup has been checked by comparing the peak 1-g SAR's for ten cellular telephones, five each at 835 and 1900 MHz, with the results obtained using a 15-tissue anatomically based model with the finite-difference time-domain (FDTD) numerical electromagnetic technique. The SAR measurement system uses a three-dimensional (3-D) stepper motor to move a Narda Model 8021 *E*-field probe to measure the SAR distribution inside a head-shaped tissue-simulant phantom near the radiating device. The head and neck part of the model with an ear-shaped protrusion of 3 mm thickness is made of a lossy outer shell of 5–7 mm thickness of epoxy laced with KCl solution. The phantom is filled with appropriate frequency-specific fluids with measured electrical properties (dielectric constant and conductivity) that are close to the average for gray and white matters of the brain at the center frequencies of interest (835 and 1900 MHz). The implantable *E*-field probe is calibrated using the FDTD-calculated SAR variations for a slab model at two commonly used frequencies, 835 and 1900 MHz and is checked to have good isotropic characteristics ( $\pm 0.23$  dB) and a wide dynamic range (0.01–10 W/kg). The system is validated using a 223-mm-diameter sphere model. Peak 1-g SAR's for ten telephones using different antennas are within  $\pm 1$  dB of those obtained using the FDTD numerical method for the anatomical model of the head and neck region.

**Index Terms**— Experimental phantom with lossy ear, safety compliance testing, validation against computed SAR.

## I. INTRODUCTION

THE use of cellular telephones and mobile wireless communication systems has increased dramatically during the past few years. Meanwhile, there is public concern for safety of RF exposure from these devices. Since the RF exposure is quantified by the mass-normalized rate of electromagnetic energy absorption or the specific absorption rate (SAR), the United States Federal Communications Commission (FCC) requires that the SAR values of new personal wireless devices must meet the prescribed RF safety guidelines [1]. Furthermore, since electromagnetic energy absorbed by the human head depends to a large extent on the antenna used for the personal wireless devices [2], knowledge of SAR distributions in the human head can also help the industry to design better antennas to improve the performance of the wireless transceivers. In this regard, we should note that 30–65% of

the power radiated by the whip antennas used today is wasted by absorption in the human head and hand [2] and this could be reduced greatly.

Recent dosimetric studies on the RF exposure to the human body from personal wireless devices have been carried out by both numerical simulation [3]–[5] and experimental measurements [6], [7]. Numerical methods using millimeter resolution anatomically based human body models and computer-aided design (CAD) files of cellular telephones can simulate the human body and the cellular phones in detail, respectively, thus providing highly accurate information about the electromagnetic coupling of the radiating device to the human body [8]. But the numerical technique requires considerable computational resources (memory and computation time) for just one test condition of the device. To alleviate this problem, use of the expanding grid finite-difference time-domain (FDTD) method [9] together with the use of the truncated models of the head [10] has resulted in savings of memory requirements by factors in excess of 20, making it possible to compute the high-resolution SAR distributions using workstations instead of parallel computers [8]. Nevertheless, if a device is to be tested for several orientations relative to the head or slightly variable conditions of the relatively unshielded internal circuitry, an easy, fast experimental procedure with validated accuracy and repeatability is of interest. A major requirement of the experimental setup, however, is that the phantom model be designed such that it gives peak 1-g SAR's that are in good agreement (within  $\pm 1$  dB) with the values obtained using anatomically based models. While none of the previously developed thin shell phantoms can make this claim in this paper, we present an automated SAR measurement system that meets this requirement and can, therefore, be used for compliance testing at both 835 and 1900 MHz. The system is fully automated by a three-dimensional (3-D) stepper motor system controlled by a computer, with a miniature implantable *E*-field probe that is used to determine spatial SAR variations. Using an ear-shaped protrusion of 3 mm thickness, the head and neck part of the phantom model is made of a lossy shell of 5–7 mm thickness of epoxy laced with KCl solution to simulate the thickness of the human skull. This is important since most of the electromagnetic energy absorption for the region of the highest SAR for anatomically based models occurs either for the ear or the internal tissues beyond the skull, which is on the order of 5–7 mm thick. This and the upper part of the torso are filled with a frequency specific fluid with measured electrical properties (dielectric constant and conductivity) close to the average properties of the brain

Manuscript received March 10, 1998; revised April 26, 1999.  
The authors are with the Department of Electrical Engineering, University of Utah, Salt Lake City, UT 84112 USA.  
Publisher Item Identifier S 0018-9375(99)06718-6.

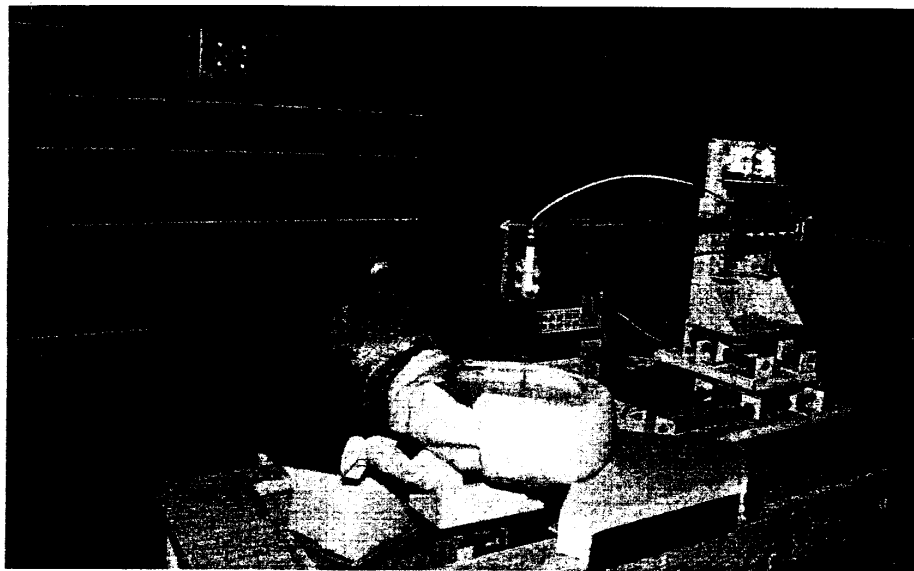


Fig. 1. Phantom model used in the automated SAR measurement system.

for white and gray matters at the center frequency of interest. Ten cellular telephones—five each at 835 and 1900 MHz with different types of antennas—have been measured for peak 1-g SAR's using this system. As desired, agreement with the FDTD calculated 1-g SAR's using an anatomically based model of a male adult is within  $\pm 1$  dB.

## II. EXPERIMENTAL SETUP AND MEASUREMENTS

### A. Experimental Setup

A photograph of the phantom model together with the computer controlled 3-D stepper motor system (Arrick Robotics MD-2A) is shown in Fig. 1. A triaxial Narda Model 8021  $E$ -field probe is used to determine the internal electric fields. The positioning repeatability of the stepper motor system moving the  $E$ -field probe is within  $\pm 0.1$  mm. Outputs from the three channels of the  $E$ -field probe are dc voltages, the sum of which is proportional to the square of the internal electric fields ( $|E_i|^2$ ) from which the SAR can be obtained from the equation  $SAR = \sigma(|E_i|^2)/\rho$ , where  $\sigma$  and  $\rho$  are the conductivity and mass density of the tissue-simulant material, respectively [11]. The dc voltages for the three channels of the  $E$ -field probe are read by three HP 34401A multimeters and sent to the computer via an HPIB interface. The setup is carefully grounded and shielded to reduce the noise due to the electromagnetic interference (EMI).

The topography of the internal surface of the phantom is prescanned with a high resolution of  $2 \text{ mm} \times 2 \text{ mm}$  so that the computer knows how far it can move the probe in the vertical direction ( $y$ ) at each horizontal position ( $x, z$ ) without breaking the probe. For scanning of the contours of the internal surface, a thin copper tape is applied to the internal surface of the phantom. Then a metal rod with the same shape and diameter as the  $E$ -field probe is moved by the stepper motor

TABLE I  
DESIRED TISSUE PROPERTIES AND THE MEASURED ELECTRICAL PROPERTIES OF THE TISSUE-SIMULANT MATERIALS FOR THE PHANTOM MODEL

	Desired*		Measured	
	$\epsilon_r$	$\sigma$ (S/m)	$\epsilon_r$	$\sigma$ (S/m)
	835 MHz			
Brain	45.3	0.92	$41.1 \pm 1.4$	$1.06 \pm 0.05$
Skull	17.4	0.25	7.4	0.16
	1900 MHz			
Brain	43.2	1.29	$45.5 \pm 1.7$	$1.31 \pm 0.06$
Skull	16.4	0.45	7.4	0.34

\*From C. Gabriel [12]

system on a programmed path to detect the surface area of dimensions  $4.8 \text{ cm} \times 14.4 \text{ cm}$  including the region of the ear and above the ear and the region of the cheek since various devices result in the highest SAR's for any of these regions. When the metal rod's tip touches the surface, an electrical signal is sent to the computer, the computer stops the stepper motor and records the position ( $x, y, z$ ). Since the positions of the stepper motor system and the phantom are relatively stable, prescanning of the phantom surface is needed only once for either the right-eared or the left-eared phantom model.

The compliance testing procedure consists of two steps. A coarser sampling with a step size of 8 mm is done in the first instance to locate the peak SAR region. The peak SAR region is then sampled with a finer step size of 2 mm on a 3-D grid over a  $1 \text{ cm}^3$  volume cube, i.e., a total of  $5 \times 5 \times 5$  points. Since the dipole sensors of the Narda Model



TABLE II  
COMPOSITION USED FOR BRAIN EQUIVALENT MATERIALS

835 MHz		1900 MHz	
Water	40.4%	Water	60.0%
Sugar	56.0%	Sugar	18.0%
Salt (NaCl)	2.5%	PEP	20.0%
HEC	1.0%	Salt (NaCl)	0.4%
		TX 151	1.6%
$\epsilon_r = 41.1 \pm 1.4$		$\epsilon_r = 45.5 \pm 1.7$	
$\sigma = 1.06 \pm 0.05$ S/m		$\sigma = 1.31 \pm 0.06$ S/m	

8021  $E$ -field probe are recessed about 4 mm from the tip of the probe, it is necessary to use an extrapolation subroutine to extend the SAR's measured in depth ( $y$ ) for each of the ( $x, z$ ) positions to the internal surface of the phantom ( $y = 0$ ) as these SAR's are generally the highest and contribute the most to the peak 1-g SAR's. We have found that a second-order polynomial obtained by using the least mean square error method is adequate and, as can be seen from the data given in Tables IV and V, gives peak 1-g SAR's that are generally within  $\pm 10\%$  of the FDTD calculated results. The whole testing procedure takes about 20 min with coarser and finer sampling steps taking about 10 min each, so the measurement can be finished within the battery charge life of most personal wireless devices.

### B. Phantom Model

The phantom model is shown in Fig. 1. The head of the phantom model has an axial length of 26 cm from the chin to the top of the head; the distance from location of the ear canal to top of the head is 14.7 cm and the width from side to side is 16.5 cm. These dimensions are typical for adult human beings. Similar to the thickness of the human skull, the head and neck part of the model is made of an outer shell of 5–7 mm thickness of epoxy laced with KCl solution for losses, except that the protruding ear region is somewhat thinner and only about 3 mm thick and this region is filled with lossy tissue-simulant material. In this regard, this phantom model is different from the thin shell models using either lossless solid plastic ears or equivalent spacers that have been used in the past [6], [7]. This and the upper part of the torso are filled with appropriate frequency-specific fluids with measured electrical properties (dielectric constant and conductivity) close to the average properties of the brain for white and gray matters at the center frequencies of interest. Table I shows the desired tissue properties [12] and the measured electrical properties of the skull-and brain-simulant materials at 835 and 1900 MHz. The head and neck region of the phantom is filled with brain simulating fluids of compositions given in Table II. A semi-solid composition of water, salt, polyethylene powder, and a gelling agent TX151 that simulates the dielectric properties equivalent to those of two-thirds muscle is used to fill a thin surgical rubber glove to create the shape of the hand. As

TABLE III  
LONG-TERM STABILITY OF THE PHANTOM MATERIAL AT 1900 MHz

Day	$\epsilon_r$	$\sigma$ (S/m)
1	$46.2 \pm 1.1$	$1.35 \pm 0.03$
7	$44.9 \pm 1.7$	$1.29 \pm 0.06$
15	$44.2 \pm 1.8$	$1.25 \pm 0.05$

shown in Fig. 1, the "hand" thus created is used to hold the cellular telephone, which is positioned against the phantom head along the line connecting the ear canal and the mouth of the phantom. This is done in order to load the handset similar to the dielectric loading provided by the hand in actual use of a hand-held wireless device.

Two different fluids of compositions given in Table II are used to simulate the average dielectric properties of the brain at 835 and 1900 MHz. The clear fluid used at 835 MHz is a composition of water, sugar, salt, and a gelling agent HEC proposed by Hartsgrave *et al.* [13]. Even without salt, this composition has an electrical conductivity  $\sigma = 1.65$  S/m, which is considerably higher than  $\sigma = 1.29$  S/m needed to simulate the average properties for the gray and white matters of the brain at 1900 MHz [12]. Thus, we have developed another liquid brain simulating material for SAR measurements at 1900 MHz. The composition of this material is also given in Table II. The dielectric properties of this material were measured using a HP 85070B dielectric probe measurement system and are given in Table II. The brain-simulant composition for use at 1900 MHz has shown a very good long-term stability (Table III) when it is properly sealed after each of the measurements to minimize the evaporation of water.

### C. E-Field Probe

The nonperturbing implantable  $E$ -field probe used in the setup was originally developed by Bassen *et al.* [14] and is now manufactured by L3/Narda Microwave Corporation, Hauppauge, NY as Model 8021  $E$ -field probe. In the probe, three orthogonal miniature dipoles are placed on a triangular-beam substrate. Each dipole is loaded with a small Schottky diode and connected to the external circuitry by high resistance ( $2 \text{ M}\Omega \pm 40\%$ ) leads to reduce secondary pickups. The entire structure is then encapsulated with a low dielectric constant insulating material. The probe thus constructed has a very small diameter (4 mm), which results in a relatively small perturbation of the internal electric field.

1) *Test for Square-Law Region:* It is necessary to operate the  $E$ -field probe in the square-law region for each of the diodes so that the sum of the dc voltage outputs from the three dipoles is proportional to the square of the internal electric field ( $|E_i|^2$ ). Fortunately, the personal wireless devices induce SAR's that are generally less than 5–6 W/kg even for closest locations of the head [2]. For compliance testing it is therefore

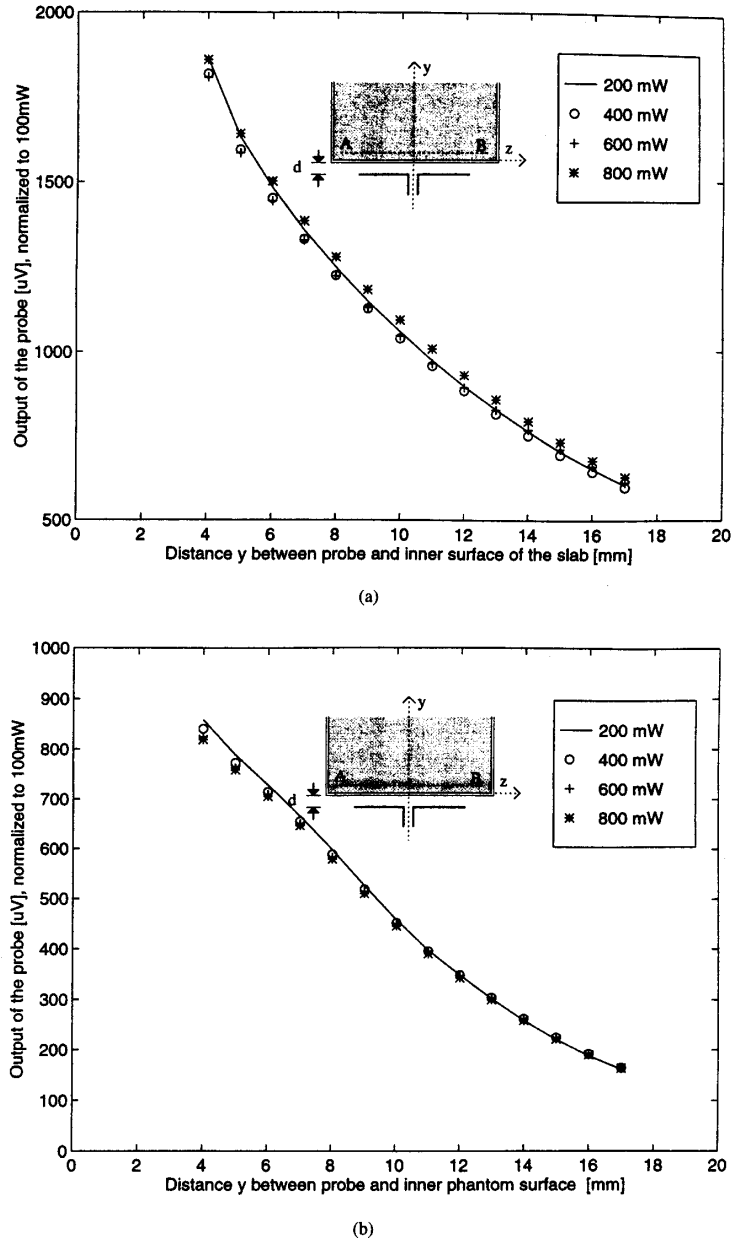


Fig. 2. Variation of the output voltage (proportional to  $|E_i|^2$ ) for different radiated powers normalized to 0.1 W. (a) Test for square-law behavior at 835 MHz. (b) Test for square-law behavior at 1900 MHz.

necessary that the  $E$ -field probe be checked for square-law behavior for SAR's up to such values that are likely to be encountered. Such a test may be conducted using a canonical lossy body, e.g, a rectangular box or a sphere irradiated by a dipole. By varying the radiated power of the dipole, the output of the probe should increase linearly with the applied power for each of the test locations.

Shown in Fig. 2(a) and (b) are the results of the tests performed to check the square-law behavior of the  $E$ -field

probe used in our setup at 835 and 1900 MHz, respectively. For these measurements we have used a rectangular box of external dimensions  $30 \times 15.5 \times 50$  cm that was irradiated by the corresponding half-wave dipoles with different amounts of radiated powers from 200–800 mW. This box of thickness 0.635 cm was filled to a depth of 13 cm with corresponding brain-simulant fluids (Table II). Used for radiators were nominal half-wave length dipoles of lengths 178 and 77 mm at 835 and 1900 MHz, respectively. Since the dc voltage outputs

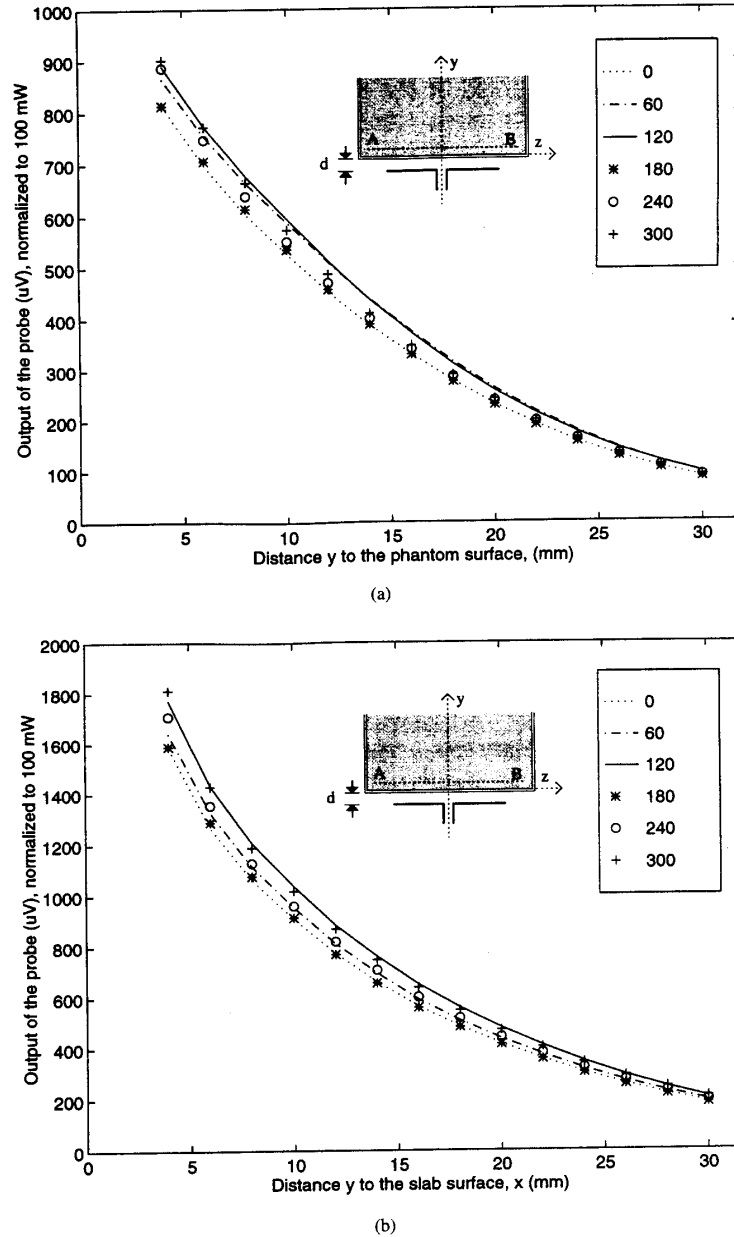
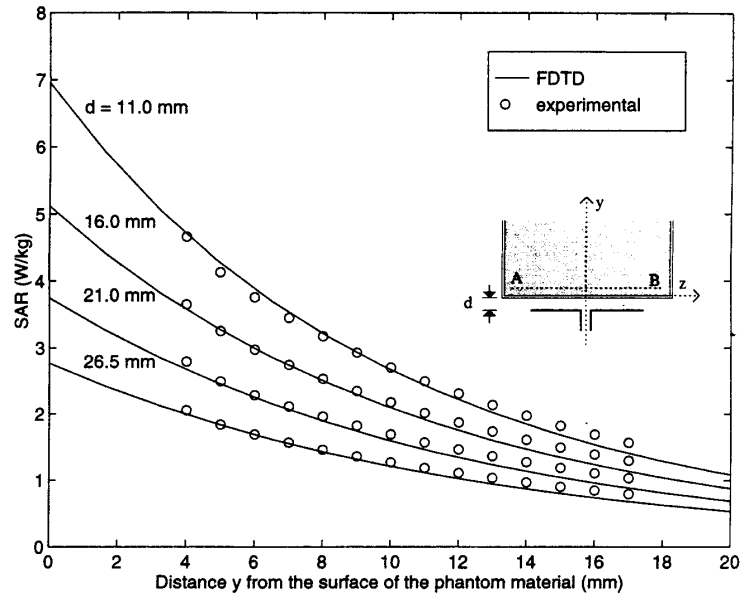


Fig. 3. (a) Test for isotropy at 835 MHz. (b) Test for isotropy at 1900 MHz.

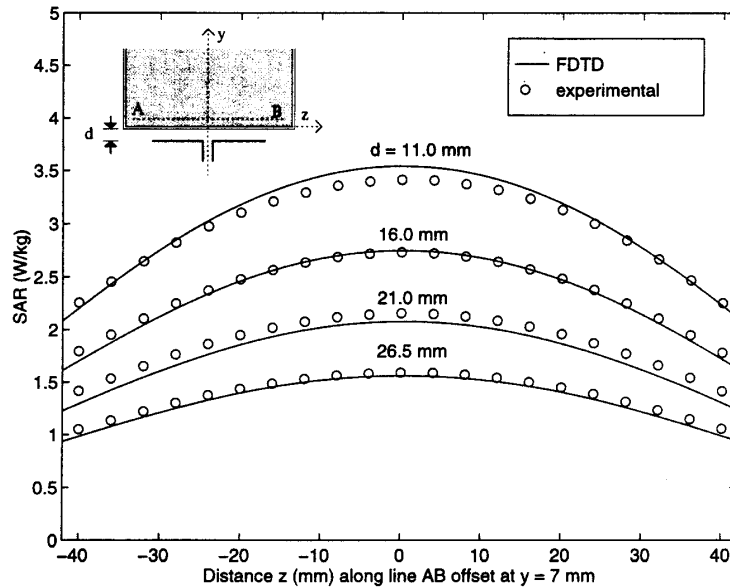
of the probe are fairly similar when normalized to a radiated power of 100 mW, the square-law behavior is demonstrated and an output voltage that is proportional to  $|E_i|^2$  is obtained within  $\pm 3\%$ .

2) *Test for Isotropy of the Probe:* Another important characteristic of the probe that affects the measurement accuracy is its isotropy. Since the orientation of the induced electric field is generally unknown, the  $E$ -field probe should be relatively isotropic in its response to the orientation of the  $E$ -field. Shown in Fig. 3(a) and (b) are the test results of the  $E$ -field

probe used in our setup at 835 and 1900 MHz, respectively. The previously described box phantom of thickness 0.635 cm and external dimensions  $30 \times 15.5 \times 50$  cm along  $x$ ,  $y$ , and  $z$  dimensions, respectively, was used for these measurements. Also used for these measurements were the two half-wavelength dipoles described above at 835 and 1900 MHz, respectively. The  $E$ -field probe was rotated around its axis from  $0$ – $360^\circ$  in incremental steps of  $60^\circ$ . As seen in Fig. 3(a) and (b), an isotropy of less than  $\pm 0.23$  dB ( $\pm 5.5\%$ ) was observed for this  $E$ -field probe both at 835 and 1900 MHz.



(a)



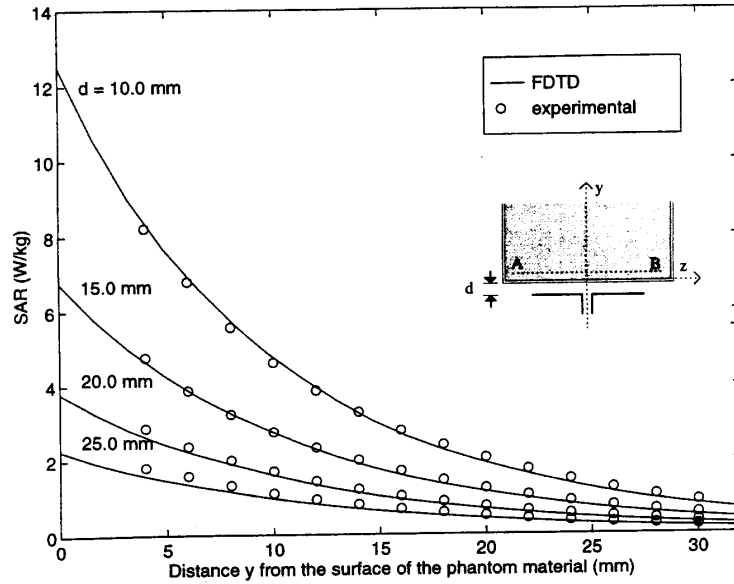
(b)

Fig. 4. Comparison of the calculated and measured SAR variations for a box phantom of external dimensions  $30 \times 15.5 \times 50$  cm; 835 MHz;  $\lambda/2$  dipole antenna; 0.5-W radiated power. Calibration factor for the Narda Model 8021 probe at 835 MHz =  $0.39$  (mW/kg)/ $\mu$ V. Measured for the phantom material  $\epsilon_r = 41.1$ ,  $\sigma = 1.06$  S/m. (a) Variation of SAR along the  $y$  axis. (b) For a line AB parallel to the  $z$  axis at a distance  $y = 7$  mm from the surface of the phantom material.

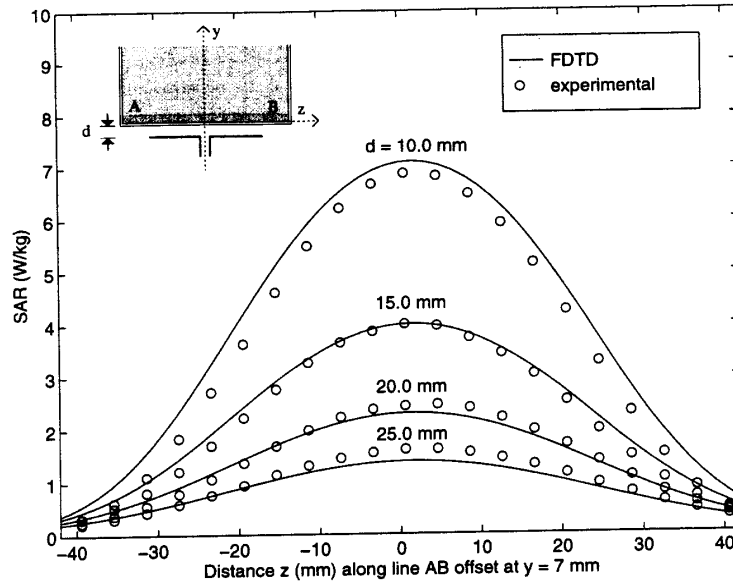
3) *Calibration of the E-field Probe:* Since the voltage output of the  $E$ -field probe is proportional to the square of the internal electric field ( $|E_i|^2$ ), the SAR is, therefore, proportional to the voltage output of the  $E$ -field probe by a proportionality constant  $C$ . The constant  $C$  is defined as the calibration factor and is frequency and material dependent. It is measured to calibrate the probe at the various frequencies of

interest using the appropriate tissue-simulating materials for the respective frequencies.

Canonical geometries such as waveguides, rectangular slabs, and layered or homogeneous spheres have, in the past, been used for the calibration of the implantable  $E$ -field probe [15]–[17]. Since the FDTD method has been carefully validated to solve electromagnetic problems for a variety of



(a)



(b)

Fig. 5. Comparison of the calculated and measured SAR variations for a box phantom of external dimensions  $30 \times 15.5 \times 50$  cm; 1900 MHz;  $\lambda/2$  dipole antenna; 0.5 W radiated power. Calibration factor for the Narda Model 8021 probe at 1900 MHz =  $0.565$  (mW/kg)/ $\mu$ V. Measured for the phantom material. (a) Variation of SAR along the  $y$  axis. (b) For a line AB parallel to the  $z$  axis at a distance  $y = 7$  mm from the surface of the phantom material.

geometries [18], [19], we were able to calibrate the Narda  $E$ -field probe by comparing the measured variations of the probe voltage ( $\propto |E_z|^2$ ) against the FDTD calculated variations of SAR's for a box phantom of external dimensions  $30 \times 15.5 \times 50$  cm used previously for the data given in Figs. 2 and 3, respectively. For these measurements, we placed the nominal half-wave dipoles of lengths 178 and 77 mm at 835 and

1900 MHz, respectively, at several distances  $d$  [see inserts of Figs. 4(a), (b) and 5(a), (b)] from the outer surface of the acrylic, ( $\epsilon_r = 2.56$ ) box of thickness 6.35 mm. Shown in Figs. 4(a) and (b) and 5(a) and (b) are the comparisons between the experimentally measured and FDTD-calculated variations of the SAR distributions in the tissue-simulant fluid for this box phantom made of an acrylic base and sides. Since

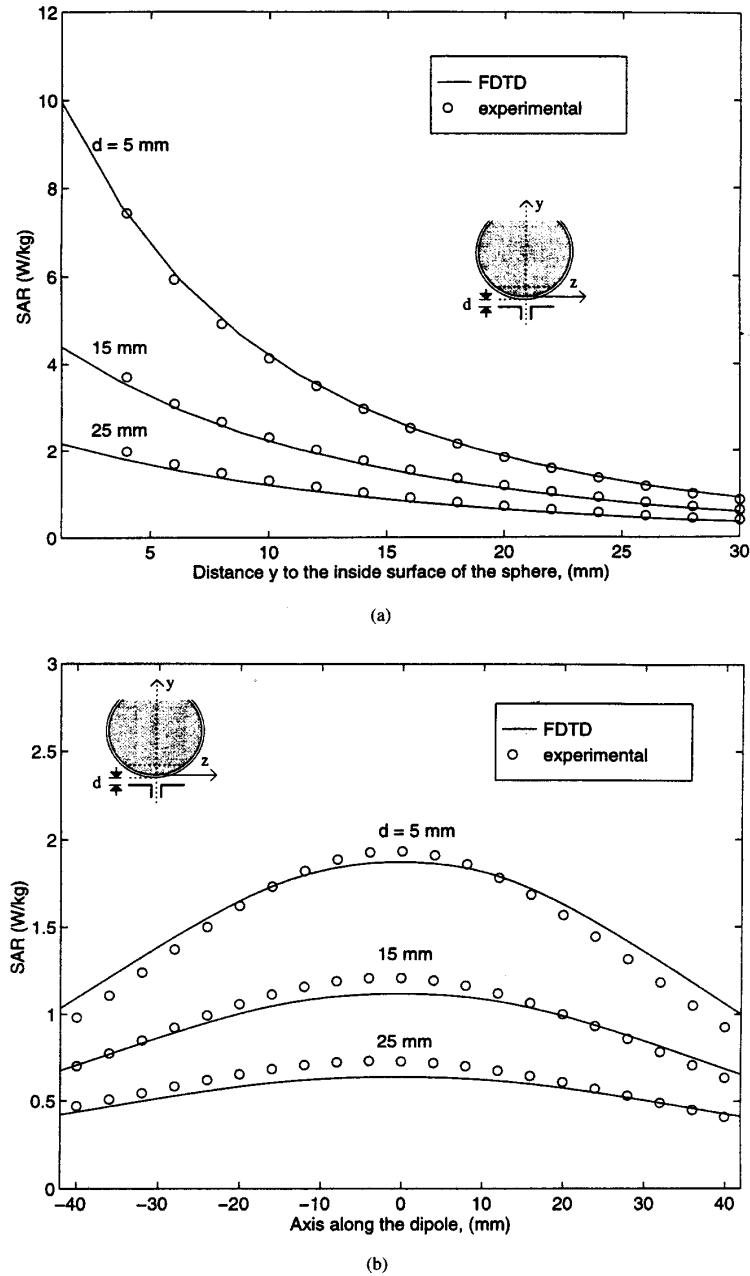


Fig. 6. Comparison of measured and FDTD calculated SAR variations at 835 MHz for a glass sphere model of outer diameter 22.3 cm and thickness 5 mm. SAR's normalized to a radiated power of 0.5 W. (a) Variation of SAR along the  $y$  axis. (b) For a plane at a distance of 20 mm from the lowest point on the inside of the sphere.

there are excellent agreements between the calculated SAR's and the measured variations of the voltage output of the  $E$ -field probe for four different separations  $d$  of the half-wave dipoles at each of the two frequencies, it is possible to calculate the calibration factors at the respective frequencies by fitting the measured data to the FDTD calculated results by means of the least mean square error method. For the Narda Model 8021  $E$ -field

probe used in our setup, the calibration factors are determined to be 0.39 and 0.565 (mW/kg)/ $\mu$ V at 835 and 1900 MHz, respectively. It should be recognized that there would be some variability in the sensitivity of the diodes used for the various units of the Narda Model 8021  $E$ -field probes. This calibration procedure using a box phantom may, therefore, be used to obtain the new calibration factors for each of the  $E$ -field probes.

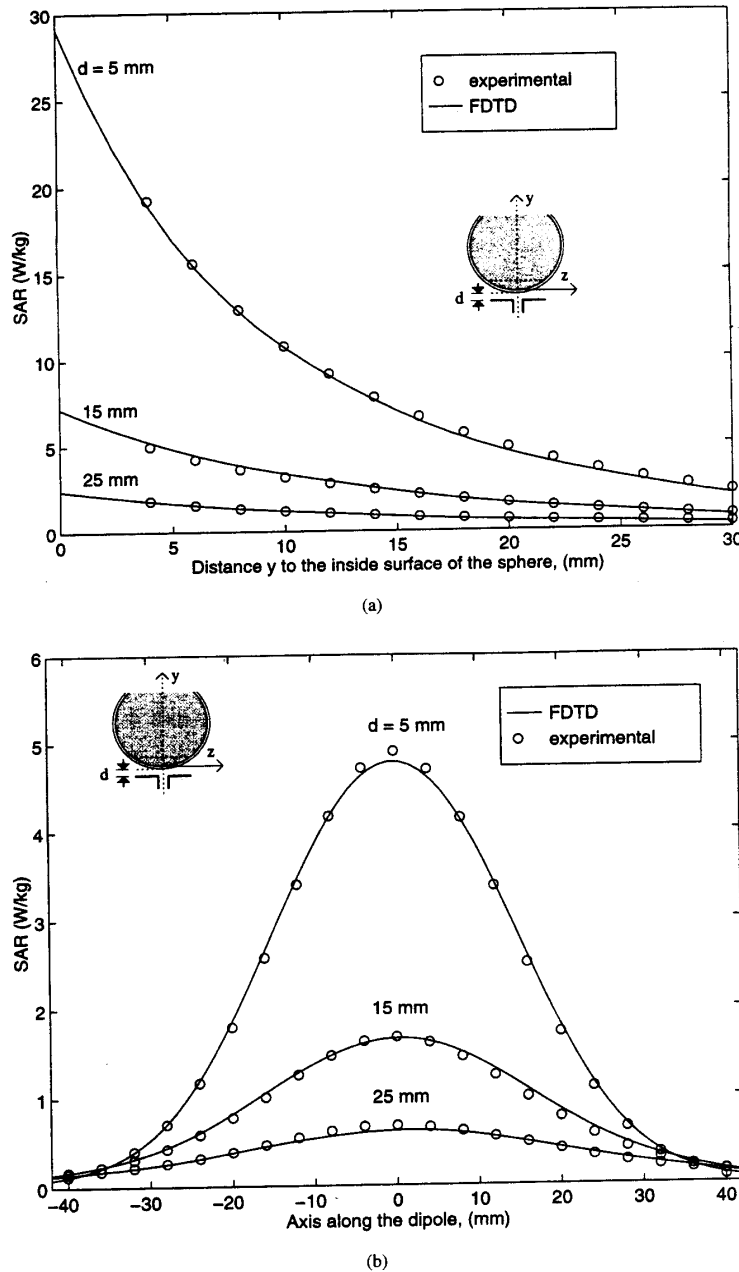


Fig. 7. Comparison of measured and FDTD calculated SAR variations at 1900 MHz for a glass sphere model of outer diameter 22.3 cm and thickness 5 mm. SAR's normalized to a radiated power of 0.5 W. (a) Variation of SAR along the  $y$  axis. (b) For a plane at a distance of 20 mm from the lowest point on the inside of the sphere. SAR's normalized to a radiated power of 0.5 W. Calibration factor =  $0.565 \text{ (mW/kg)/}\mu\text{V}$ . Measured for the phantom material  $\epsilon_r = 45.5$ ,  $\sigma = 1.31 \text{ S/m}$ .

### III. EXPERIMENTAL RESULTS: CANONICAL PROBLEMS

To further validate the SAR measurement system, it has been used to measure the peak 1-g SAR for the abovementioned box phantom and a glass sphere model of thickness 5 mm, external diameter = 223 mm and dielectric constant  $\epsilon_r = 4.0$ . This sphere model is once again filled with the

corresponding brain-simulant fluids of compositions given in Table II at 835 and 1900 MHz, respectively. Shown in Figs. 6(a) and (b) and 7(a) and (b) are the measured and FDTD calculated SAR distributions inside the sphere for various separations  $d$  between the dipole and the sphere (see insert for Figs. 6 and 7). Comparison of the measured and FDTD-

TABLE IV  
BOX PHANTOM:  
COMPARISON OF THE MEASURED AND FDTD CALCULATED PEAK 1-g SAR'S FOR  
FOUR SPACINGS EACH AT 835 AND 1900 MHz RADIATED POWER NORMALIZED TO 0.5 W

Frequency (MHz)	Distance (mm) between $\lambda/2$ dipole and the Box	SAR (W/kg)		Difference (%)
		Measured	FDTD	
835	17.5	4.58	4.20	+8.3
835	22.5	3.53	3.65	-3.4
835	27.5	2.69	3.00	-10.2
835	33.0	1.95	2.24	-12.9
1900	16.5	7.45	7.46	-0.1
1900	21.5	4.24	4.18	+1.4
1900	26.5	2.71	2.91	-7.9
1900	31.5	1.77	1.75	+1.1

TABLE V  
SPHERE PHANTOM:  
COMPARISON OF THE MEASURED AND FDTD-CALCULATED PEAK 1-g SAR'S FOR THREE  
SPACINGS EACH AT 835 AND 1900 MHz, RADIATED POWER NORMALIZED TO 0.5 W

Frequency (MHz)	Distance (mm) between $\lambda/2$ dipole and the sphere	SAR (W/kg)		Difference (%)
		Measured	FDTD	
835	5	6.78	6.77	+0.23
835	15	3.41	3.27	+4.22
835	25	1.85	1.68	+9.51
1900	5	17.45	18.01	-3.21
1900	15	4.96	5.05	-1.81
1900	25	1.69	1.77	-4.73

calculated peak 1-g SAR's for both phantom geometries are given in Tables IV and V, respectively. As can be seen, the agreement between experimental measurement and numerical simulation is very good and generally within  $\pm 10\%$  for both the rectangular and spherical phantoms.

#### IV. SAR MEASUREMENTS FOR CELLULAR TELEPHONES

The automated setup shown in Fig. 1 has been used for testing of ten personal wireless devices five each at 835 and 1900 MHz, respectively. Given in Table VI is the comparison of the numerical and measured peak 1-g SAR's for these devices using our experimental phantom model and the FDTD-based numerical procedure used for calculations of SAR distributions for an anatomically based model of the head of an adult male. The procedure for determining the peak 1-g SAR using the FDTD method with anatomical model has previously

been detailed in our earlier publications [2], [10]. Like the experimental method, it too relies on the determination of the averaged SAR for a volume of dimensions approximately  $1 \times 1 \times 1$  cm with a mass as close to 1 g as possible. The measured and calculated SAR's for the ten telephones, which have quite different operational modes (time division multiple access [TDMA] or code division multiple access [CDMA]) and antenna structures (helical, monopole, or helix-monopole) vary from 0.13 to 5.41 W/kg. Even though widely different peak 1-g SAR's are obtained because of the variety of antennas and handsets, agreement between the calculated and the measured data is good and generally within  $\pm 20\%$  ( $\pm 1$  dB). This is remarkable since a magnetic resonance image (MRI) derived, 15-tissue anatomically based model of the adult human head is used for FDTD calculations and a relatively simplistic two tissue phantom model is used for experimental peak 1-g SAR measurements. It is interesting to note that even



TABLE VI  
COMPARISON OF THE EXPERIMENTALLY MEASURED AND FDTD-CALCULATED PEAK 1-g SAR'S  
FOR TEN COMMERCIAL WIRELESS DEVICES, FIVE EACH AT 835 AND 1900 MHz, RESPECTIVELY

	Time-Averaged Radiated Power mW	Experimental Method W/kg	Numerical Method W/kg
Cellular Telephones at 835 MHz			
Telephone A	600	4.02	3.90
Telephone B	600	5.41	4.55
Telephone C	600	4.48	3.52
Telephone D	600	3.21	2.80
Telephone E	600	0.54	0.53
PCS Telephones at 1900 MHz			
Telephone A'	125	1.48	1.47
Telephone B'	125	0.13	0.15
Telephone C'	125	0.65	0.81
Telephone D'	125	1.32	1.56
Telephone E'	99.3	1.41	1.25

though the dielectric properties of the external shell (Fig. 1) are not as high as for the living human skull (see Table I), the peak 1-g SAR's obtained with this experimental phantom model agree quite well for the ten telephones used to date for which both the numerical and experimental procedures have been used.

#### V. CONCLUSIONS

An automated SAR measurement system has been developed with a dynamic range (0.01–10 W/kg) suitable for the compliance testing of personal wireless devices. This system uses a thick lossy shell of KCl-laced epoxy of 3–7 mm thickness to simulate the thickness of the human skull in the region of the maximum SAR's, i.e., the ear and the cheek. Unlike the previously reported thin-shell lossless ear phantoms [6], [7], the accuracy of this experimental phantom has been checked by comparing the peak 1-g SAR's for ten cellular telephones, five each at 835 and 1900 MHz, with the 1-g SAR's obtained using a 15-tissue anatomically based model with the FDTD numerical electromagnetic technique. Peak 1-g SAR's for these ten telephones using monopole, helix, or helix-monopole antennas are within  $\pm 1$  dB of those obtained using the FDTD method for the anatomical model of the human body [2].

#### ACKNOWLEDGMENT

The authors would like to thank Dr. G. Lazzi and Dr. A. Tinniswood for their many helpful discussions and the FDTD calculations.

#### REFERENCES

- [1] FCC 96-326, "Guidelines for evaluating the environmental effects of radio frequency radiation," FCC, Washington, DC 20554, Aug. 1, 1996.
- [2] O. P. Gandhi, G. Lazzi, and C. M. Furse, "Electromagnetic absorption in the human head and neck for mobile telephones at 835 and 1900 MHz," *IEEE Trans. Microwave Theory Tech.*, vol. 44, pp. 1884–1897, Oct. 1996.
- [3] G. Lazzi and O. P. Gandhi, "On modeling and personal dosimetry of cellular telephone helical antennas with the FDTD code," *IEEE Trans. Antennas Propagat.*, vol. 46, pp. 525–529, Apr. 1998.
- [4] O. P. Gandhi and J. Y. Chen, "Electromagnetic absorption in the human head from experimental 6-GHz transceivers," *IEEE Trans. Electromagn. Compat.*, vol. 37, pp. 547–558, Nov. 1995.
- [5] M. A. Jensen and Y. Rahmat-Samii, "EM interaction in handset antennas and a human in personal communications," *Proc. IEEE*, vol. 83, pp. 7–17, Jan. 1995.
- [6] Q. Balzano, O. Garay, and T. J. Manning, Jr., "Electromagnetic energy exposure of simulated users of portable cellular telephones," *IEEE Trans. Veh. Technol.*, vol. 44, pp. 390–403, 1995.
- [7] T. Schmid, O. Egger, and N. Kuster, "Automated E-field scanning system for dosimetric assessments," *IEEE Trans. Microwave Theory Tech.*, vol. 44, pp. 105–113, Jan. 1996.
- [8] A. D. Tinniswood, C. M. Furse, and O. P. Gandhi, "Computations of SAR distributions for two anatomically-based models of the human head using CAD files of commercial telephones and the parallelized FDTD code," *IEEE Trans. Antennas Propagat.*, vol. 46, pp. 829–833, June 1998.
- [9] B. Q. Gao and O. P. Gandhi, "An expanding-grid algorithm for the finite-difference time-domain method," *IEEE Trans. Electromagn. Compat.*, vol. 34, pp. 277–283, Aug. 1992.
- [10] G. Lazzi and O. P. Gandhi, "Realistically tilted and truncated anatomically-based models of the human head for dosimetry of mobile telephones," *IEEE Trans. Electromagn. Compat.*, vol. 39, pp. 55–61, Feb. 1997.
- [11] M. A. Stuchly and S. S. Stuchly, "Experimental radio and microwave dosimetry," in *Handbook of Biological Effects of Electromagnetic Fields*, 2nd ed., C. Polk and E. Postow, Eds. Boca Raton, FL: CRC, 1996, pp. 295–336.
- [12] C. Gabriel, "Compilation of the dielectric properties of body tissues at RF and microwave frequencies," U.S. Air Force Armstrong Laboratory, Rep. AL/OE-TR-1996-0037, Brooks Air Force Base, TX 78235, June 1996.
- [13] G. Hartsgrove, A. Kraszewski, and A. Surowiec, "Simulated biological materials for electromagnetic absorption studies," *Bioelectromagn.*, vol. 8, pp. 29–36, 1987.
- [14] H. I. Bassen and G. S. Smith, "Electric field probes 3/4 a review," *IEEE Trans. Antennas Propagat.*, vol. AP-3, pp. 710–718, Sept. 1983.
- [15] D. Hill, "Waveguide techniques for the calibration of miniature electric field probes for use in microwave bioeffects studies," *IEEE Trans. Microwave Theory Tech.*, vol. MTT-30, pp. 92–94, 1982.
- [16] N. Kuster and Q. Balzano, "Energy absorption mechanism by biological bodies in the near field of dipole antennas above 300 MHz," *IEEE Trans. Veh. Technol.*, vol. 41, pp. 17–23, Feb. 1992.
- [17] M. A. Stuchly, S. S. Stuchly, and A. Kraszewski, "Implantable electric field probes—Some performance characteristics," *IEEE Trans. Biomed. Eng.*, vol. BME-31, pp. 526–531, July 1984.

- [18] A. Taflove, K. R. Umashankar, and T. G. Jurgens, "Validation of FDTD modeling of the radar cross section of three-dimensional structures spanning up to nine wavelengths," *IEEE Trans. Antennas Propagat.*, vol. AP-33, pp. 662-666, June 1985.
- [19] C. M. Furse, Q. Yu, and O. P. Gandhi, "Validation of the finite-difference time-domain method for near-field bioelectromagnetic simulations," *Microwave Opt. Technol. Lett.*, vol. 16, pp. 341-345, Dec. 1997.



**Qishan Yu** was born in Shandong, China, in 1967. He received the B.S. and M.S. degrees in physics from Peking University, China, in 1985 and 1992, respectively.

Since 1996, he has been a graduate student in the Electrical Engineering Department, University of Utah, Salt Lake City, and has worked as a Research Assistant in the Bioelectromagnetics Laboratory, Electrical Engineering Department, at the same university.



**Om P. Gandhi** (M'58-SM'65-F'79-LF'99) is a Professor and the Chairman of the Department of Electrical Engineering, University of Utah, Salt Lake City. He is the author or coauthor of several book chapters and journal articles on electromagnetic dosimetry, microwave tubes, and solid-state devices. He also recently edited *Biological Effects and Medical Applications of Electromagnetic Energy* (Englewood Cliffs, NJ: Prentice-Hall, 1990) and coedited *Electromagnetic Biointeraction* (New York: Plenum, 1989).

Dr. Gandhi received the Distinguished Research Award from the University of Utah (1979-1980) and a special award for Outstanding Technical Achievement from the IEEE, Utah Section, in 1975. He has been co-chairman of IEEE SCC 28.IV subcommittee on RF safety standards (1988-1997), served as Vice President/President of the Bioelectromagnetics Society (1991-1993), and as chairman of the IEEE Committee on Man and Radiation (COMAR) (1980-1982). In 1995 he received the d'Arsonval Medal of the Bioelectromagnetics Society for pioneering contributions to the field of bioelectromagnetics. He is listed in *Who's Who in the World*, *Who's Who in America*, *Who's Who in Engineering*, and *Who's Who in Technology Today*.



**Magnus Aronsson** (S'96) was born in Stockholm, Sweden, on March 25, 1973. He received the B.S. degree (*magna cum laude*) in electrical engineering from the University of Utah, Salt Lake City, in 1997. He is currently pursuing the M.S. degree in electrical engineering at the same university.

Since 1997, he has been a Research Assistant at the bioelectromagnetics group, University of Utah.

**Ding Wu**, photograph and biography not available at the time of publication.

## APPENDIX B

### **Uncertainty Analysis**

The uncertainty analysis of the University of Utah SAR Measurement System is given in Table A.1. Several of the numbers on tolerances are obtained by following procedures similar to those detailed in [8], while others have been obtained using methods suggested in [4].

Table B.1. Uncertainty analysis of the University of Utah SAR Measurement System.

Uncertainty Component	Tolerance ± %	Prob. Dist.	Div.	C <sub>i</sub> 1-g	1-g u <sub>i</sub> ± %
<b>Measurement System</b>					
Probe calibration	2.0	N	1	1	2.0
Axial isotropy	4.0	R	√3	(1-c <sub>p</sub> ) <sup>1/2</sup>	1.6
Hemispherical isotropy	5.5	R	√3	√c <sub>p</sub>	0.0
Boundary effect	0.8	R	√3	1	0.5
Linearity	3.0	R	√3	1	1.7
System detection limits	1.0	R	√3	1	0.6
Readout electronics	1.0	N	1	1	1.0
Response time	0.0	R	√3	1	0.0
Integration time	0.5	R	√3	1	0.3
RF ambient conditions	0	R	√3	1	0
Probe positioner mechanical tolerance	0.5	R	√3	1	0.3
Probe positioning with respect to phantom shell	2.0	R	√3	1	1.2
Extrapolation, interpolation, and integration algorithms for max. SAR evaluation	5.0	R	√3	1	2.9
<b>Test Sample Related</b>					
Test sample positioning	3	R	√3	1	1.7
Device holder uncertainty	3	R	√3	1	1.7
Output power variation - SAR drift measurement	5	R	√3	1	2.9
<b>Phantom and Tissue Parameters</b>					
Phantom uncertainty - shell thickness tolerance	10.0	R	√3	1	5.8
Liquid conductivity - deviation from target values	0.4	R	√3	0.7	0.2
Liquid conductivity - measurement uncertainty	1.5	R	√3	0.7	0.6
Liquid permittivity - deviation from target values	0.8	R	√3	0.6	0.3
Liquid permittivity - measurement uncertainty	3.5	R	√3	0.6	1.2
<b>Combined Standard Uncertainty</b>		RSS			8.3
<b>Expanded Uncertainty (95% Confidence Level)</b>					16.6